JOURNAL OF CATALYSIS 109, 143–155 (1988)

The Oxidation of Ethylene over Silver-Based Alloy Catalysts

4. Silver–Zinc Alloys

NOREDDINE TOREIS,* XENOPHON E. VERYKIOS,*,[1] SYED M. KHALID,† GRANT BUNKER,† AND Z. RICHARD KORSZUN†

*Department of Chemical Engineering, Drexel University, and †University City Science Center, Institute for Structural and Functional Studies, Philadelphia, Pennsylvania 19104

Received November 13, 1986; revised August 4, 1987

Silver–zinc alloy catalysts were prepared by impregnation of α-alumina supports with mixed silver nitrate and zinc nitrate solutions. They were characterized in terms of exposed metallic surface area and surface composition, employing selective chemisorption of oxygen and hydrogen. A dramatic enrichment of the surface with Zn was observed and was not altered after exposure of catalysts to reaction conditions. XPS analysis indicates that surface Zn atoms are in the 2+ valence state. Kinetic parameters of ethylene epoxidation and combustion were found to be nearly unaffected by the presence of Zn atoms on the surface of the catalysts. EXAFS analysis indicates that silver atoms exhibit absorption characteristics which are nearly identical to atoms in a silver foil, which was used as a standard. Thus, silver atoms are coordinated mostly to other silver atoms, indicating that Ag–Zn clusters consist of a central core of primarily silver atoms with Zn atoms primarily on the surface.

INTRODUCTION

The effects of geometric and electronic factors in catalysis by alloy or bimetallic catalysts were investigated with silver-based alloys under ethylene oxidation conditions. Ethylene oxidation was selected as a probe reaction because the structural sensitivity of kinetic parameters is well established in this system (*1–3*). Furthermore, there are reasons to believe that this reaction is also sensitive to the electronic structure of catalytic surfaces. The mode of oxygen adsorption, in terms of its atomic or diatomic nature, appears to play a major role in mechanistic and kinetic factors. The dissociative or nondissociative adsorption of oxygen on silver is expected to be influenced significantly by the electronic structure of its surface since the electron transfer requirements of the two processes are different.

The alloying metals selected for this study are palladium and gold, whose electronegativities are higher than that of silver, cadmium and zinc, whose electronegativities are lower than that of silver. Other criteria applied in this selection included bulk composition range in which monophasic alloys can be achieved, expected surface composition range, and thermodynamics of alloy formation.

In previous publications (*4–6*), the effects of alloying silver with palladium, cadmium, and gold on kinetic parameters in ethylene epoxidation and combustion were presented. In the case of Ag–Pd alloy catalysts, turnover frequency of epoxidation was found to decrease, while that of combustion was found to increase with increasing Pd content. Activation energies of both reactions were found to be independent of surface composition. In the case of Ag–Cd alloy catalysts, turnover frequency of epoxidation was found to increase with increas-

[1] Present address: Institute of Chemical Engineering and High-Temperature Chemical Processes, Department of Chemical Engineering, University of Patras, Patras, Greece.

0021-9517/88 $3.00

ing Cd content of the surface, while that of combustion was found to be nearly independent of surface composition. Activation energies of both reactions, especially that of the epoxidation, were found to decrease with increasing Cd content. Over Ag–Au alloy catalysts, both specific rates exhibited maxima at a surface composition of 10–15 atom% Au, while catalytic activity was totally eliminated over surfaces containing 30% or more Au.

These results were interpreted primarily in terms of near-neighbor electronic interactions between dissimilar atoms (atoms with different electronegativity), affecting the electron structure of surface silver atoms and in terms of geometric alterations of surfaces. In the present communication the effects of alloying silver with zinc on kinetic parameters in ethylene oxidation are presented. Zn is of the same electronegativity relative to silver as cadmium, therefore, qualitatively similar results would be expected, if indeed electronic interactions are responsible for observed alterations in catalytic performance of silver.

EXPERIMENTAL

Supported silver–zinc alloy catalysts were prepared with bulk compositions in the range 0–20 atom% Zn. Monometallic catalysts of Ag and Zn were also prepared, all with a metal loading of 5 wt%. The support employed was α-alumina of low surface area (Carborundum, SAHT-99) crushed to a particle size between 0.1 and 0.4 mm. Catalysts were prepared by simultaneous impregnation of the support with known amounts of mixed silver nitrate and zinc nitrate solutions of appropriate concentration. The volume of the solution used was in slight excess of the pore volume of the support. The impregnated supports were then dried in an oven overnight at 100°C and reduced in flowing hydrogen for 24 h at 200°C. By means of a General Electric counter diffractometer with Ni-filtered Cu$K\alpha$ radiation, catalysts were examined with respect to alloying achieved by X-ray diffraction. Scanning was performed between 30 and 80° (2θ).

Total surface area was obtained by the BET method, using argon as adsorbate at the temperature of liquid nitrogen. The exposed metallic surface area of the catalysts and the surface composition of the alloy particles were determined by selective chemisorption of oxygen and hydrogen. Adsorption experiments were conducted in a constant-volume high-vacuum apparatus (Micromeritics, Accusorb 2100E) which achieves a dynamic vacuum of 10^{-6} mm Hg. Selective chemisorption of oxygen was conducted at 200°C at O_2 pressures up to 25 mmHg and of hydrogen was conducted at 220°C at H_2 pressures up to 100 mm Hg. Experimental details and surface pretreatment procedures have been reported elsewhere (*4*, *5*).

Kinetic parameters were obtained in an isothermal, packed-bed, tubular reactor, in the temperature range 217–235°C, at a pressure of 15 atm. The feed composition consisted of 3.0% ethylene, 3.3% oxygen, and 93.7% nitrogen. Oxygen concentration was kept at low levels to prevent phase separation of the alloy catalysts during reaction. Further details of kinetic experiments have been reported in an earlier publication (*4*).

X-ray absorption spectra were measured on the C2 beamline of the Cornell High-Energy Synchrotron Source (CHESS). The electron beam energy and current were 5.3 Gev and ~25 mA, respectively. Silicon (111) crystals were used. All measurements were made in the transmission mode with an argon-filled ion chamber as the incident flux monitor and a xenon-filled sealed ion chamber to measure the transmitted intensity. The sample edge steps were less than 1.5 $\Delta\mu x$ to minimize problems from thickness effects.

Samples, in fine powder form, were pressed inside brass cartridges of 1 cm inside diameter. The large amount of sample used eliminated the possibility of pin holes and other nonuniformities. Sample car-

tridges were precooled in liquid nitrogen and placed inside a copper pipe immersed in a liquid nitrogen bath. Ends were capped with styrofoam to minimize frosting. The X-ray beam was transmitted along the axis of the cylinder through the sample.

The amount of catalyst used in sample preparation was determined on the basis of equal surface density with the standard. A double fold of a commercially available (AESAR) Ag foil of 13 μm thickness was used as a standard. Surface density was computed by

$$W_d = \frac{\Delta \ln(I_0/I)}{W_m[(\mu/\rho)_a - (\mu/\rho)_b]} \qquad (1)$$

where W_d is surface density (g/cm^2), I_0 is the incident flux, recorded in the front ion chamber, and I is the flux recorded at the back ion chamber, after absorption. W_m is the weight fraction of the element under investigation, while $(\mu/\rho)_a$ and $(\mu/\rho)_b$ are the X-ray absorption coefficients above and below the absorption edge (Ag–K edge), respectively. Values of 55.21 and 9.2 cm^2/g were assumed (*7*). Application of Eq. 1 to the standard Ag foil gives a surface density of 27.3 mg/cm^2. Since the catalyst samples consisted of 4 wt% Ag, a total surface density of 683 mg/cm^2 is required, which corresponds to a silver surface density of 27.3 mg/cm^2, identical to that of the standard. Problems with "thickness" effects are avoided by choosing an appropriate sample thickness (in the vicinity of one absorption length). By matching the absorption of standard and unknown, residual thickness effects tend to cancel. This is not a major problem in this work, however, because of the low level of harmonic radiation at the energies used.

Data analysis was done following standard procedures (*8*), which include normalization to unit edge step, conversion from energy to X-ray wavenumber K, background subtraction by means of a four-region cubic spline function, Fourier transform, and filtering. The energy zero was taken at the midpoint of the edge. Signals from higher shells damp out more rapidly with K than that of the first shell because of their larger Debye–Waller factors. To enhance the contributions of higher shells relative to the first shell, the transform range was restricted to $3.3 < K < 11.9$ Å^{-1}. The backscattering amplitude and phase for atoms of high Z, such as silver, exhibit considerable structure, which introduces side lobes and peak splitting in the transforms if not divided out beforehand. The experimentally determined amplitude and phase for the first shell of Ag foil were divided (or subtracted) out of the catalyst data prior to transformation. Because of this division no additional K weighting was necessary. A strongly tapered (4 Å^{-1} width at each window edge) Hanning K-space window was then applied to minimize truncation ripple. These precautions minimize spurious structure in the Fourier transforms from the amplitude and phase modulation.

RESULTS AND DISCUSSION

Examination of phase diagrams of Ag–Zn alloys indicates that monophasic random solutions can be obtained up to a Zn content of 30 atom%. To ensure that monophasic alloy catalysts were used in this study, the maximum zinc content of alloys used was 20 atom%. Catalysts were also subjected to X-ray diffraction analysis before and after exposure to reaction conditions. Diffraction peaks from a number of crystal planes were recorded and lattice constants were obtained by plotting $\cos^2\theta$ versus a_0 and extrapolating to $\theta = 90°$. Lattice constants thus obtained are shown in Fig. 1 as a function of bulk alloy composition. These results compare favorably with those reported in the literature (*9*), which are also shown on the same figure. The small differences can probably be attributed to the fact that the results of this study are based on small supported alloy particles while those of Ref. (*9*) are based on bulk alloys. X-ray diffraction analysis of catalysts after exposure to reaction condi-

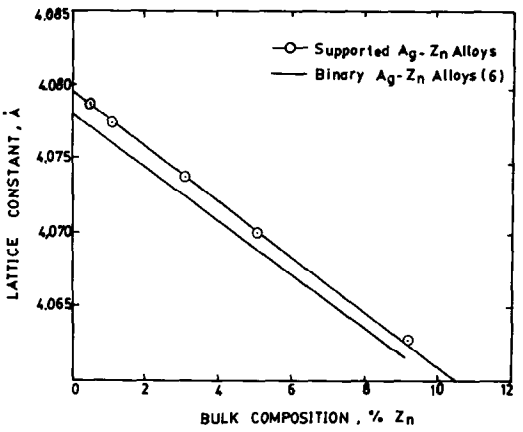

FIG. 1. Lattice constants of Ag–Zn alloys as a function of bulk composition.

tions indicated no phase separation of the alloys during reaction.

Surface Composition of Ag–Zn Alloy Particles

The fact that surface composition can differ substantially from bulk composition in equilibrated alloys has been demonstrated theoretically and experimentally (*10, 11*). An experimental scheme based on selective chemisorptive titrations was developed to determine surface composition of alloy particles as a function of bulk composition. The technique was verified in preliminary experiments employing argon physisorption and oxygen and hydrogen chemisorption on pure zinc powders, zinc dust, and supported zinc crystallites. Results are summarized in Table 1. The good agreement in exposed surface area of zinc powder and zinc dust obtained with argon physisorption and oxygen chemisorption at 200°C indicates that oxygen adsorption can be used to determine the number of surface atoms. It is well-known that monolayer coverage of silver surfaces can also be obtained with oxygen at 200°C. Therefore, oxygen chemisorption can be used to determine the total number of exposed atoms of Ag–Zn alloy particles since O_2 does not adsorb on α-Al_2O_3 supports at this temperature.

Hydrogen chemisorption on Zn/α-Al_2O_3 samples was investigated in the temperature range 100–220°C in two samples of different metal loading. Results shown in Table 1 indicate that the amount of hydrogen adsorbed increases with increasing temperature. The amount of hydrogen adsorbed at 220°C, in both cases, is in good agreement with the amount of oxygen adsorbed at 200°C, indicating that monolayer coverage of Zn surfaces with hydrogen is achieved at 220°C. The increase of the amount of hydrogen adsorbed with increasing temperature is probably due to a kinetic effect, in which case the results obtained at lower temperatures do not correspond to true isotherms. Hydrogen was found not to adsorb on silver or α-Al_2O_3, to any measurable extent, at 220°C.

On the basis of these preliminary investigations, surface composition of supported Ag–Zn alloy catalysts was determined by selective oxygen chemisorption at 200°C, from which the total number of exposed metal atoms is estimated, and by selective chemisorption of hydrogen at 220°C, from which the number of surface Zn atoms is determined. Typical oxygen and hydrogen adsorption isotherms on Ag–Zn alloy catalysts are shown in Figs. 2 and 3, respectively. Small differences in the oxygen adsorption isotherms (Fig. 2) correspond to small differences in dispersion. The total

TABLE 1

Comparative Results of Preliminary Chemisorptions Experiments

Adsorbent	Adsorbate	Temperature (°C)	Exposed area (m^2/g)
Zn powder	Ar	−196	0.169
Zn powder	O_2	200	0.175
Zn dust	Ar	−196	0.130
Zn dust	O_2	200	0.134
Zn/Al_2O_3	H_2	100	0.009
Zn/Al_2O_3	H_2	210	0.020
Zn/Al_2O_3	H_2	220	0.032
Zn/Al_2O_3	O_2	200	0.031
Zn/Al_2O_3	H_2	200	0.055
Zn/Al_2O_3	H_2	220	0.062
Zn/Al_2O_3	O_2	200	0.064

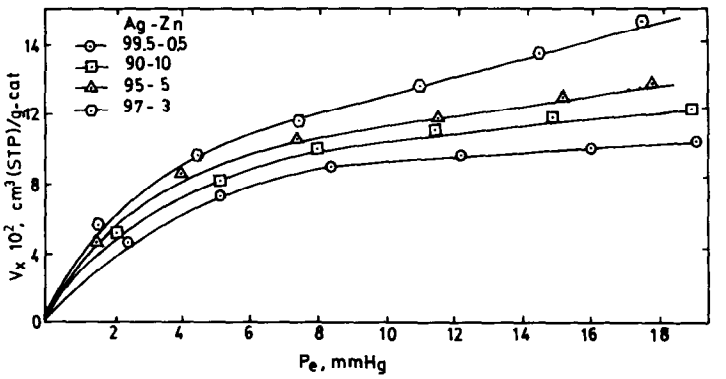

FIG. 2. Oxygen adsorption isotherms on supported Ag–Zn alloy catalysts at 200°C.

exposed metallic area of all catalysts used in this study was found to be between 0.29 and 0.32 m^2/g, varying randomly with composition within this range. Differences in hydrogen adsorption isotherms (Fig. 3) correspond to differences in the number of Zn atoms on the surface of the alloy particles. As expected, the amount of hydrogen adsorbed increases with increasing Zn content of the alloys.

A problem which this particular alloy system presents is associated with the fact that Zn can be oxidized very easily during chemisorption experiments, under reaction conditions or even during exposure to ambient conditions. Thus, it is quite possible that surface zinc is present in the form of ZnO. To address this question, high-resolution ESCA was performed on a sample containing 5% Zn–95% Ag, before and after exposure to reaction conditions. ESCA scans were obtained for C 1*s*, Zn $2p^3$ and Ag $3d^5/3d^3$ photoelectron lines. The Zn $L_3M_{45}M_{45}$ Auger band was also recorded and is shown in Fig. 4. The shapes of the zinc Auger bands and the equivalent Auger binding energies indicate that Zn is in the 2+ valence state in both samples. Therefore, surface zinc atoms get oxidized when exposed even to atmospheric oxygen and remain in that state during reaction. Then, the chemisorption techniques described above determine the number of ZnO molecules on the surface of the alloy particles. Adsorption stoichiometry does not present a problem since the state of the samples used in "calibration" experiments was the same as that of the actual samples.

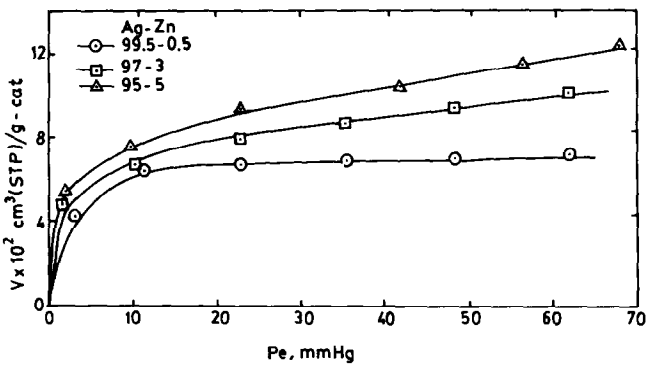

FIG. 3. Hydrogen adsorption isotherms on supported Ag–Zn alloy catalysts at 220°C.

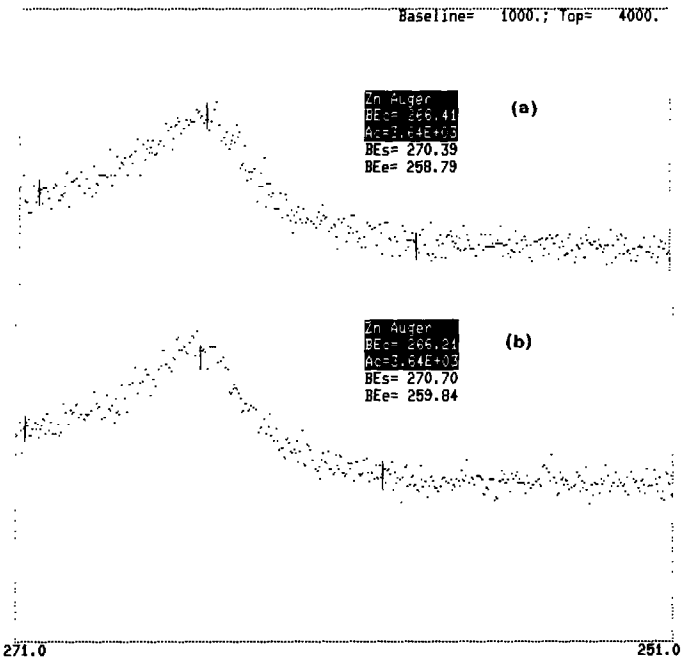

FIG. 4. Zinc Auger bands of (a) fresh and (b) used catalyst (5% Zn–95% Ag).

Surface composition of supported Ag–Zn alloy particles as a function of bulk compositions is shown in Fig. 5. Two sets of experimental points are shown, one indicating surface composition before catalysts were exposed to reaction conditions and one developed from used catalysts. In addition, a theoretical curve, based on the model of Williams and Nason (*12*), is shown in the same figure. This model of surface compo-

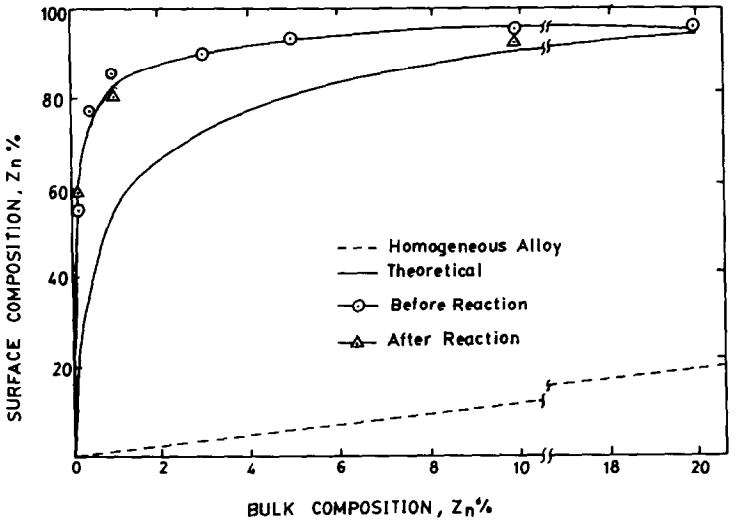

FIG. 5. Surface composition of supported Ag–Zn alloy catalysts as a function of bulk composition.

sition of alloys is based on thermodynamic properties of individual components and was developed by minimizing alloy surface energy under the regular solution approximation. Both experimental and theoretical curves show a dramatic enrichment of the surface with Zn, the component with the lower heat of sublimation, a phenomenon which has also been observed in other alloy systems (*4, 5, 10*).

The degree of surface enrichment with Zn, determined experimentally, is higher than what the theoretical model predicts. This is due to the fact that the theoretical model is based on the assumption that the alloy is at equilibrium with vacuum. It is well known that the environment in which the alloy exists can influence surface composition significantly. If the alloy exists at equilibrium with a particular gaseous atmosphere, the component with the higher heat of adsorption and higher heat of formation of the metal–gas bond tends to accumulate at the surface, a phenomenon referred to as chemisorption-induced surface enrichment. During adsorption the alloys were exposed to oxygen. Zn–O bonds have a heat of formation significantly higher than that of Ag–O bonds. During both preparation and adsorption, the alloys were exposed to hydrogen, which adsorbs on Zn but only negligibly on Ag. All these factors favor higher enrichment of the surface with Zn, as the experimental curve in Fig. 5 indicates. It must also be noted that surface composition is not measurably altered after catalysts are exposed to reaction conditions. This is in agreement with XPS analysis, which shows that surface Zn atoms are already in the 2+ valence state before exposure to reaction conditions; therefore, no further rearrangement of surface atoms occurs. Total metallic surface area of alloys was also found to be the same in fresh and spent catalysts.

Kinetic Parameters

Specific rates per exposed silver atom (turnover frequencies) of ethylene epoxidation and combustion reactions were determined with an isothermal reactor operated in the differential mode, utilizing surface compositions obtained from selective chemisorption experiments (Fig. 5). Preliminary experiments conducted with supported Zn catalysts indicated that Zn does not exhibit any catalytic activity under the conditions employed in this study. Thus, turnover frequencies were computed in terms of the silver component only and any changes in kinetic parameters can be attributed to some type of interaction between Ag and ZnO atoms at the surface of the catalyst.

Turnover frequencies of epoxidation and combustion reactions are shown as a function of surface composition (in atom% Zn) of the alloy catalysts on Fig. 6. Both specific rates increase very slightly with increasing Zn content of the surface. As a result, selectivities, shown in Fig. 7 as a function of surface composition, are nearly independent of Zn content of the surface. The same is true of activation energies, especially of the combustion reaction. Activation energy of the epoxidation reaction is shown in Fig. 7 to decrease slightly with increasing Zn content of the surface. The activation energy of the epoxidation reaction is found to be in the neighborhood of 21 kcal/mol while that of the combustion reaction is approximately 25 kcal/mol, in agreement with other studies (*1, 4, 5*).

In previous publications from this laboratory (*4–6*) the effects of alloying Ag with Pd, Cd, and Au atoms on kinetic parameters in ethylene oxidation were presented. In the case of Ag–Cd alloy catalysts, specific epoxidation rates were found to increase substantially with increasing Cd content of the surface, while rates of combustion were found to be nearly unaffected by alloying. Activation energies of both reactions were found to decrease with increasing surface Cd concentration, with the activation energy of epoxidation decreasing significantly more rapidly. These observations were explained in terms of geometric

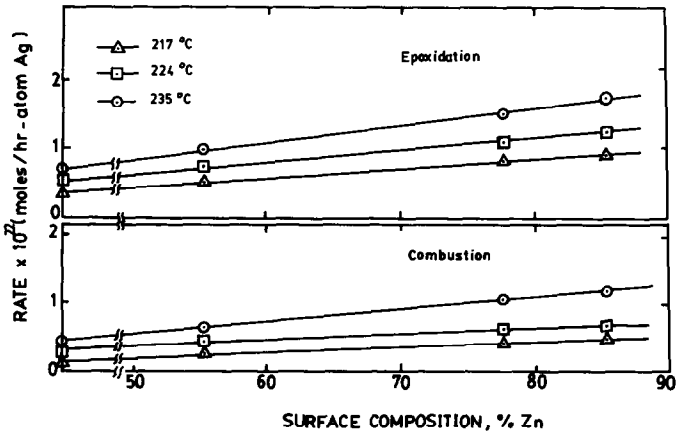

FIG. 6. Variation of turnover frequencies of epoxidation and combustion with surface composition.

and primarily electronic interactions between Ag and Cd atoms. If indeed near-neighbor electronic interactions are responsible for the observed alterations of kinetic parameters when Ag is alloyed with Cd, then qualitatively similar results would be expected from the Ag–Zn catalytic system since Zn is of the same electronegativity relative to Ag as Cd. Nevertheless, experimental observations do not support this premise.

To explain this apparent discrepancy, extended X-ray absorption fine structure (EXAFS) analysis of supported Ag–Zn and Ag–Cd alloy catalysts were conducted. Both samples consisted of 80 atom% Ag and 20 atom% of alloying metal. Results are compared with spectra obtained with a sil-

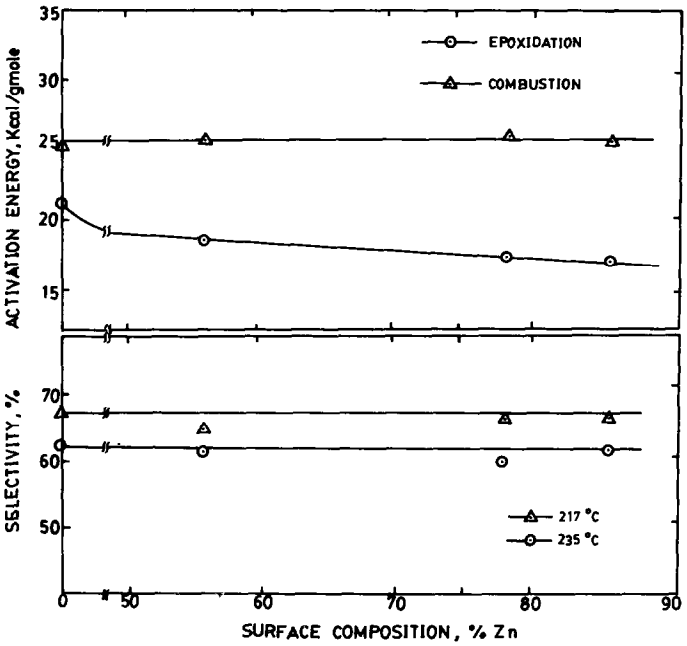

FIG. 7. Variation of activation energies and selectivity with surface composition.

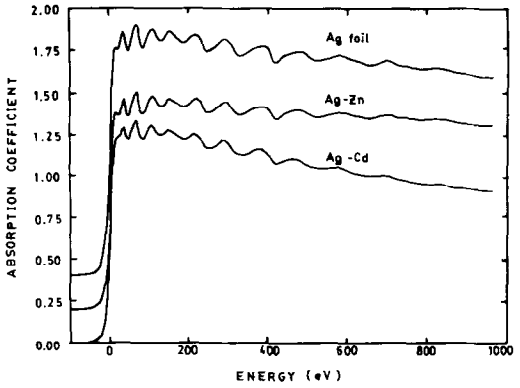

FIG. 8. *K*-edge spectra of Ag foil, Ag–Zn, and Ag–Cd at 80 K.

ver foil used as a standard. The EXAFS spectra were measured at 80 K for the silver *K*-edge of the catalysts and the standard. *K*-edge absorption spectra of silver

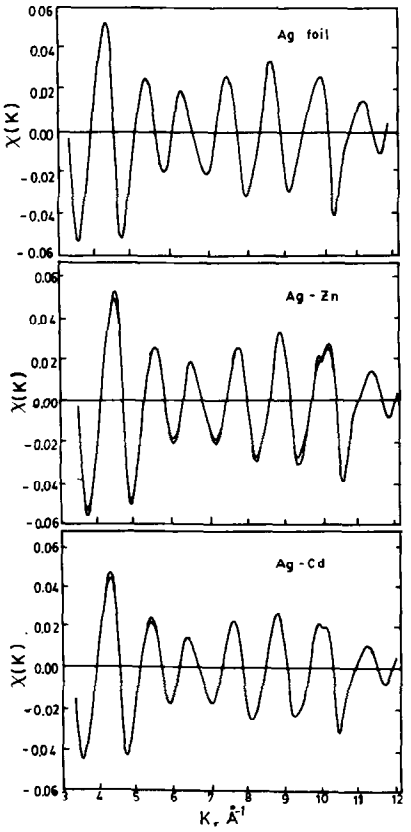

FIG. 9. EXAFS spectra of Ag in Ag foil, Ag–Zn, and Ag–Cd at 80 K.

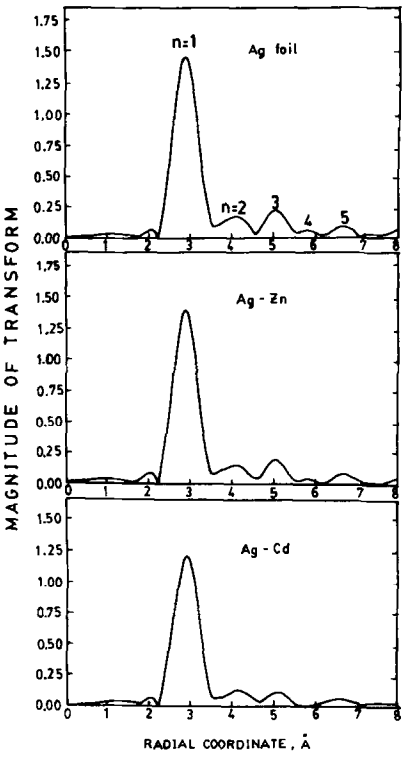

FIG. 10. Phase- and amplitude-corrected Fourier transforms of EXAFS spectra of Ag foil, Ag–Zn, and Ag–Cd.

foil, Ag–Zn and Ag–Cd are shown in Fig. 8, and corresponding EXAFS functions, $\chi(K)$ versus K are shown in Fig 9. As described under Experimental, phase- and amplitude-corrected Fourier transforms of the $\chi(K)$ functions were taken over the range of wave vectors, **K**, of 3.3 to 11.9 $Å^{-1}$ and are shown in Fig. 10.

A close inspection of silver EXAFS results of the Ag–Zn catalyst reveals that both the $\chi(K)$ function and its corrected Fourier transform are essentially identical to those of Ag in the silver foil; they can practically be superimposed. This observation indicates that the environment about a silver atom in Ag–Zn alloy particles is, on the average, not different from that in the reference foil. Furthermore, matching of the Fourier transform functions occurs at even higher radial distances, indicating that even higher shells are identical. The aver-

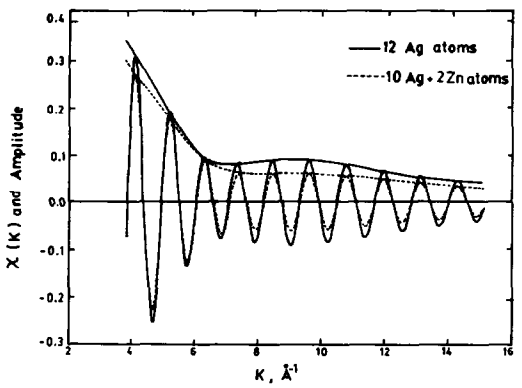

FIG. 11. EXAFS spectra and amplitude envelopes of Ag in environments of 12 Ag and 10 Ag + 2 Zn atoms, using Teo's and Lee's (*12*) synthesis.

age radial distance between Ag atoms and their nearest neighbors was also determined from the EXAFS data. In the Ag–Zn catalyst, the nearest-neighbor distance of silver was found to be 2.89 Å, equal to that of the standard Ag foil.

The results discussed above are consistent with a view in which a silver–zinc cluster consists of a central core of primarily silver atoms with zinc atoms present primarily at the surface of the cluster. Similar results have been obtained on Ru–Cu and Os–Cu alloy particles supported on silica (*13*) and were interpreted in a similar manner. Further evidence of this structural arrangement is obtained by theoretical analysis of EXAFS functions of pure silver (12 atoms considered) and silver atoms in a random solid solution with zinc (10 Ag and 2 Zn atoms). These theoretical EXAFS functions were synthesized with the scattering amplitudes and phases of Teo and Lee (*14*) and results are presented in Fig. 11 as $\chi(K)$ versus K as well as amplitude envelopes. The bond lengths for both Ag and Zn were taken as those in the silver foil, 2.89 Å. Even if the Zn atoms are substituted for Ag, significant differences in $\chi(K)$ would be expected. EXAFS spectra of silver coordinated to Zn in Ag–Zn alloys are expected to be significantly different from EXAFS spectra of Ag coordinated to Ag atoms only. Therefore, the only plausible explanation of the identity of EXAFS spectra of silver in silver foil and Ag–Zn particles is the structural arrangement described above in which silver is coordinated mainly to other silver atoms. This structural arrangement implies minimal, if any, geometric or electronic alterations of catalytic surfaces and, therefore, minimal effects of alloying on kinetic parameters.

An apparent contradiction between the EXAFS and XRD results is obvious. This contradiction can be resolved by the following reasoning: In a nutshell, EXAFS provides information on short-range structure; XRD provides information on long-range, crystalline order. These types of information are not equivalent. Peaks in the powder patterns show up for only well-ordered phases with domains large enough to give strong, narrow peaks. In a disordered system, large portions of the sample may be essentially invisible to XRD. On the other hand, EXAFS yields information on the short-range structure, averaged over the whole sample. One sees all atoms of the selected element, whatever the degree of order. However, EXAFS tells you very little about the long-range order (length scales greater than about 5 Å). In this respect, EXAFS and XRD are complementary.

XRD shows that the *average* lattice constant of the particle obeys Vegard's law, and no diffraction peaks corresponding to bulk Zn are observed in the powder patterns. This indicates that the surface layer of Zn (or ZnO), is thin enough that it is invisible to XRD under the conditions of the powder pattern experiment. On the other hand, the EXAFS results indicate that the Ag atoms see primarily Ag neighbors; that is, there is significant depletion of Zn in the average Ag coordination environment. This does not necessarily imply that there is bulk phase segregation of Zn. What presumably is happening is that there is a gradient in Zn concentration within the particles. Such a gradient would entail a gradient in local lattice constants. Such a gradi-

ent would not change the *average* lattice constant obtained from XRD because Vegard's law works fairly well. Furthermore, XRD samples only a small portion of the sample (since it sees only those parts with long-range order), while EXAFS samples the entire sample and proves massive segregation of Ag.

Therefore, there is a contradiction between EXAFS and XRD only if the additional (unwarranted) assumption that the particles are perfectly homogeneous (apart from possible surface layer of Zn) is made. There may be a statistical tendency for Ag and Zn to avoid each other without bulk-phase segregation occurring.

In contrast to the Ag–Zn alloy system, silver EXAFS spectra of Ag–Cd alloy particles are significantly different from silver EXAFS spectra of silver foil, indicating that the environment about a silver atom in the alloy is, on the average, different from that in the foil. In the Fourier transform plots, the amplitude of the Ag–Cd system is smaller than that of the silver foil in the main peak and in subsequent ones. A tendency for centroids to shift to a higher radial coordinate is also apparent. In the plots of EXAFS functions, $\chi(K)$ versus K, it is observed that zero nodes have the tendency to shift to lower values of K, and the difference is progressively greater as K increases. The amplitudes are smaller than the ones corresponding to silver foil. With the silver foil as a reference, the nearest-neighbor distance of silver in the Ag–Cd alloy was determined to be 2.91 Å, which is higher than that of the silver foil by 0.02 Å. Theoretical simulations show that this shift is not a consequence of the slight differences between Cd and Ag backscattering phase shifts. These results demonstrate that in Ag–Cd alloy particles, silver atoms are coordinated to Cd atoms as well as to other silver atoms, resulting in a geometric and electronic configuration different from that of pure silver particles.

Peaks in the phase- and amplitude-corrected Fourier transforms of EXAFS spectra are real since the extent of noise was determined to be significantly smaller by comparison of two scans on the same sample under same conditions. Moreover, correction for backscattering amplitude and phase functions was performed and a strongly tapered transform window was used to suppress the truncation sidelobes in the Fourier transforms. Therefore, subsequent peaks in the Fourier transform plots correspond to higher shells. The average radial distance between silver and its nearest neighbors in the nth shell were then calculated. The ratio of the average radial distance in the nth shell, r_n, to that of the first shell, r_1, was computed and is shown in Table 2. No entry is provided for the fourth shell of Ag–Cd because the Fourier transform peak that corresponds to this shell (Fig. 10), although it does exist, is so small that it can hardly be distinguished from noise. The ratio of these radial distances is found to be in good agreement with the relationship

$$r_n/r_1 = n^{1/2}, \qquad (2)$$

which is specific of an FCC structure. Thus, it can be concluded that in both Ag–Zn and Ag–Cd alloy particles the FCC structure is conserved even at higher shells. This conclusion supports the results of X-ray diffraction analysis.

Results of EXAFS analysis clearly demonstrate that the geometric and electronic structure of silver atoms in the Ag–Zn cata-

TABLE 2

Comparison of Values of r_n/r_1 and Expected Values of FCC Structure

n	$n^{1/2}$	r_n/r_1	
		Ag–Cd	Ag–Zn
2	1.41	1.42 ± 0.06	1.40 ± 0.06
3	1.73	1.75 ± 0.06	1.74 ± 0.06
4	2.00	—	1.99 ± 0.06
5	2.24	2.28 ± 0.06	2.30 ± 0.06

lysts is not significantly different from that of pure silver. It is not surprising, therefore, that significant changes in kinetic parameters of ethylene epoxidation and combustion were not detected when Ag was alloyed with Zn. It must also be emphasized that EXAFS is a bulk technique, and since the particles of the catalysts employed in this study are very large (>850 Å), results pertain to the bulk structure of these particles. Any alterations of the surface only would not be detected by EXAFS.

As chemisorption and ESCA experiments have shown, alloy surfaces contain both Ag atoms and ZnO molecules. Even if all ZnO molecules are segregated in clusters, a small fraction of Ag atoms on the surface must be coordinated to ZnO molecules. Some degree of alteration of the electron structure of these atoms is expected by near-neighbor interactions. Apparently, the fraction of surface Ag atoms which are affected by the presence of ZnO is small. As a result, the effects of such interactions on kinetic parameters are not significant. Nevertheless, a close inspection of Figs. 6 and 7 reveals that turnover frequency of epoxidation tends to increase with increasing Zn content of the surface, while activation energy tends to decrease. It must be noted that identical trends, although significantly more pronounced, were also observed in the Ag–Cd catalytic system (*5*).

In the combustion reaction, the effects of alloying silver with cadmium were significantly less pronounced than those of epoxidation. While epoxidation activity increased by a factor of three, combustion activity increased only slightly. Similarly, activation energy of epoxidation decreased by 45% while that of combustion decreased by 20%. Similar trends might be present in the Ag–Zn system but because they are less pronounced, for the reason discussed earlier, they were not detected in kinetic experiments. An increasing tendency of combustion activity with increasing Zn content is apparent in Fig. 6.

SUMMARY AND CONCLUSIONS

Silver–zinc alloy particles supported on α-alumina were employed in studies of ethylene oxidation and results are compared with those obtained over Ag–Cd alloys, since Zn and Cd are of the same electronegativity relative to Ag. Surface composition of Ag–Zn alloy particles was determined by selective chemisorption techniques and found to be dramatically different from bulk composition. Zinc atoms were found to dominate the surface and to be in the 2+ valence state even before exposure of the catalysts to reaction conditions. Kinetic parameters in ethylene epoxidation and combustion were found to be minimally affected by the presence of ZnO on catalyst surfaces. EXAFS analysis of a Ag–Zn alloy catalyst indicates that the environment of silver atoms in the alloy is not different from that of silver atoms in a silver foil which was used as a standard. Thus, Ag–Zn clusters consist of a central core of primarily silver atoms, with zinc atoms primarily on the surface. In contrast, EXAFS analysis of Ag–Cd alloy catalysts indicates that Ag atoms are coordinated to Cd as well as to Ag atoms, and, as a result, the geometric and electronic structure of the alloy is affected by near-neighbor interactions. The fact that alterations of kinetic parameters were significant when silver was alloyed with cadmium but minimal when it was alloyed with zinc is attributed to the different structural arrangement of the two alloy particles, as described above.

REFERENCES

1. Verykios, X. E., Stein, F. P., and Coughlin, R. W., *Catal. Rev. Sci. Eng.* **22,** 197 (1980).
2. Verykios, X. E., Stein, F. P., and Coughlin, R. W., *J. Catal.* **66,** 368 (1980).
3. Campbell, C. T., *J. Catal.* **94,** 436 (1985).
4. Mehrotra, P., and Verykios, X. E., *J. Catal.* **88,** 409 (1984).
5. Bonin, B. K., and Verykios, X. E., *J. Catal.* **91,** 36 (1985).
6. Toreis, N., and Verykios, X. E., *J. Catal.*, in press.
7. McMaster, W. H., Del Grande, N. K., Mallett, J. H., and Hubbell, J. H., "Compilation of X-Ray

Cross Sections." Lawrence Radiation Laboratory, UCRL-50174, Section 2, Rev. 1, 1969.
8. Sayers, D. E., Stern, E. A., and Lytle, F. W., *Phys. Rev. Lett.* **27,** 1204 (1971).
9. Pearson, W. B., "Handbook of Lattice Spacings and Structure of Metals." Pergamon, London, 1967.
10. Ponec, V., *Catal. Rev. Sci. Eng.* **11,** 41 (1975).
11. Sachtler, W. M. H., and Van Santen, R. A., *Catal. Rev. Sci. Eng.* **26,** 69 (1979).
12. Williams, F. L., and Nason, D., *Surf. Sci.* **45,** 377 (1974).
13. Sinfelt, J. H., Via, G. H., and Lytle, F. W., *Catal. Rev. Sci. Eng.* **26,** 81 (1984).
14. Teo, B. K., and Lee, P. A., *J. Amer. Chem. Soc.* **101,** 2815 (1979).